Meta-atom Microfluidic Sensor for Highly Sensitive Cell Detection

Ali Bahrami (alibahrami14@gmail.com)

Research Article

Keywords: microfluidics, split ring resonator, CTC, high sensitivity sensor, cell detection

Posted Date: March 21st, 2022

DOI: https://doi.org/10.21203/rs.3.rs-1471094/v1

Meta-atom Microfluidic Sensor for Highly Sensitive Cell Detection

Ali Bahrami

Department of Electrical Engineering, Sharif University of Technology, Tehran, Azadi Avenue, 11365/8639*, Iran*

Abstract

A meta-atom microfluidic-based sensor (MAMS) for detecting, enumerating and differentiating cancer cells is proposed. A microfluidic constriction channel is placed between the gaps of a two-gap split ring resonator (SRR). This two-gap SRR is implemented in a way that is sensitive to the stiffness of the cell which is passing through the constriction channel. With passing a cell through the channel, geometrical features of the SRR changes, and these changes are reflected in the device output. In addition, dielectric properties of the cells passing through the constriction channel, changes the sensor output upon electromagnetic excitation of the SRR. As both stiffness and relative permittivity of the cell, which are biosignatures of a cell, determines the output characteristics of the sensor, this label-free assay can almost perfectly distinguish between different cancer cells and normal cells with high sensitivity. Sensor function is simulated and analyzed, as proof of concept, to show the effectiveness and high sensitivity of the device in differentiating of cells with different dielectric and stiffness properties.

Keywords: microfluidics, split ring resonator, CTC, high sensitivity sensor, cell detection

I. Introduction

Microfluidic devices have emerged as promising technology for facilitating acquisition of novel biosignatures based on electrical and mechanical properties of cancer cells [1]. These intrinsic physical properties of cells that reflect underlying

molecular structure are indicators of cell state associated with a number of processes including cancer progression, stem cell differentiation, and drug response. Particularly, cell mechanical stiffness is an indicator of various changes in cells state including cancer cell function, motility, and invasion capacity [2]. Many tools capable of probing cell mechanics, including atomic force microscopy (AFM), optical tweezers, and magnetic tweezers, have been developed [3]. To increase the throughput, microfluidic approaches have been developed that rely on either the physical constriction or the hydrodynamic shear stress from a channel, a cross-section, or a T-junction [4]. The microfluidic constriction channel is used to quantify the cellular entry and transition process through a micro channel with a cross-sectional area smaller than the dimensions of a single cell, enabling single cell detection and enumeration [5]. The deformability of cells through constriction channels has been used to distinguish tumor cells from non-tumorigenic cells [6]. Using other cell characteristics besides mechanical properties such as optical properties simultaneously in a single assay enables very accurate cell differentiation. Split-ring resonators are ideal structures for the realization of compact high-sensitivity and high-resolution sensors due to their high-quality factor resonance, compact size, and high sensitivity to changes in the constituent materials and physical dimensions [7]. Various metamaterial-based sensors have been studied at microwave frequencies for chemical and biosensing applications, as they offer label-free measurement, less time-consuming sample preparation, low fabrication cost, and suitability for lab-on-a-chip implementation [8].

In this work, a system consisting of a microfluidic constriction channel and a two-gap SRR, for cell detection and enumeration with high sensitivity is presented. Using both dielectric properties and stiffness, as electro-optical and mechanical signatures

of a cell, is expected to provide label-free, accurate and highly sensitive biomarkers of cell type and state.

II. MAMS Structure

The structure of MAMS is shown in Fig. 1. The structure consists of a polydimethylsiloxane (PDMS) microfluidic constriction channel with cross section of 8 × 6 μm^2. Two voids (blue regions beside constriction channel in Fig. 1) as relaxation regions are also created to allow the cell to interact with and displace SRR (golden region in Fig. 1) arms (We call each side of the SRR arm) and partially recover its shape. The SRR material is gold and its width, length and thickness are 2, 25 and 0.5 μm, respectively. The SRR is placed on two supports (black regions in Fig. 1) which holds the suspended SRR (effects of mass and gravity is negligible). The SRR contains two suspended planes in the constriction channel which interact with the cell passing through the constriction channel, and act as a stiffness sensor; very stiff cells can displace the SRR arms, or equivalently change the geometrical dimensions of the SRR more than less-stiff cells and these geometrical changes are directly reflected in the output characteristics of MAMS. The gap (without displacement) between these two planes is 6 μm and its thickness is 1 μm. There are another PDMS layer on top of the structure to avoid leakage of carrier fluid to outside environment which is not shown for better visualization.

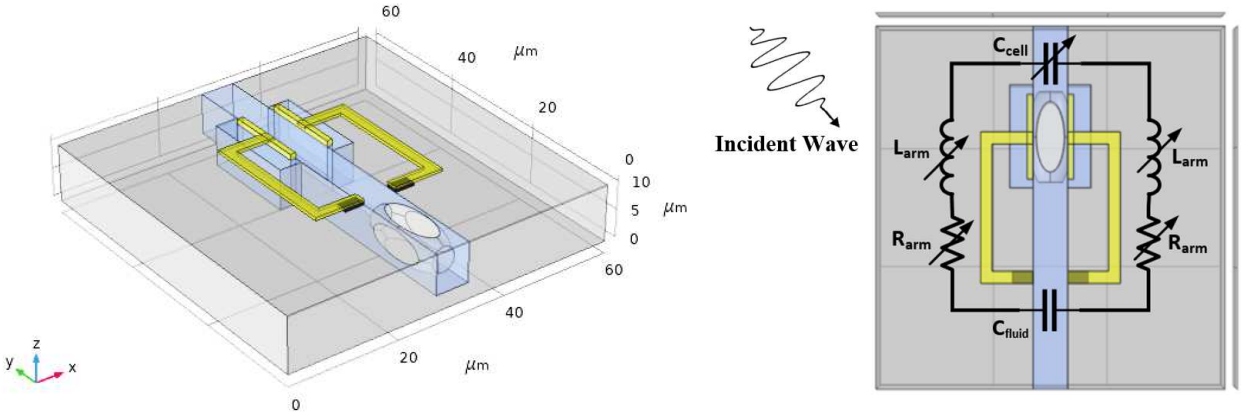

Fig. 1. MAMS structure

To calculate how much force a cell passing through the constriction channel exerts on each arm and resultant displacement of the arms, compression of spherical objects in contact with two parallel plane is calculated [9, 10]. In our simulations, it is supposed that the undeformed and unstressed cell shape is sphere. In addition, it is supposed that the geometry is symmetric about the yz plane which crosses the middle of the cell, $x = 30\ \mu m$ plane in Fig. 2(a), and therefore the arms have equal displacement.

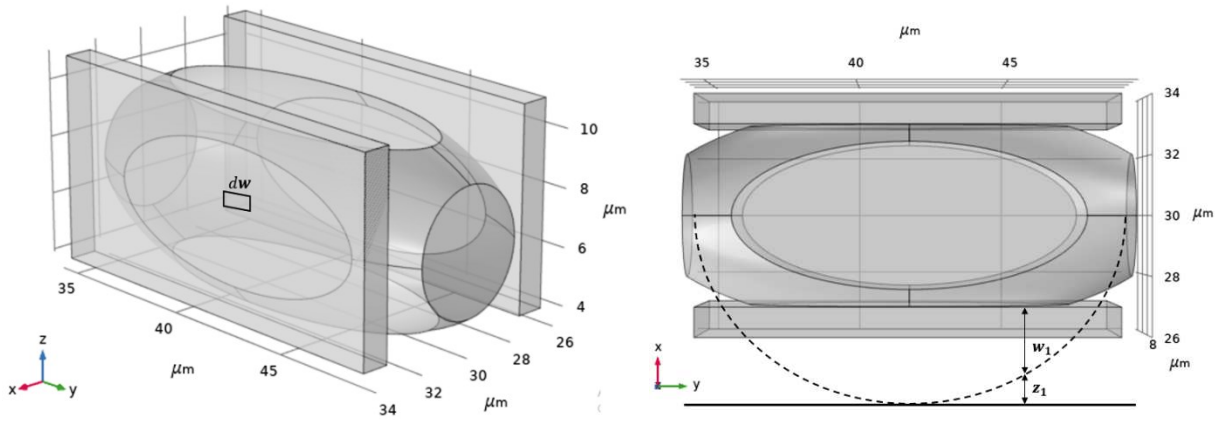

(a) (b)

Fig. 2. A squeezed cell in the constriction channel. (a) Decompression force differential element inside the area of contact. (b) Displacement of the cell at an arbitrary point inside the area of contact.

When squeezed cell is in contact with the rectangle part of the arms in the constriction channel (for the sake of simplicity, we say in contact with the arms), decompression forces displace the arms. It is supposed that the decompression forces act along x direction and other components of the force are neglected. As shown in Fig. 2(b), w_1 is the displacement of the cell at an arbitrary point inside the area of contact. Then, by considering a differential force element dw at a point (y', z') inside the area of contact, the deformation of the cell at (y, z) point is [10]:

$$w(y,z) = \frac{1-\sigma^2}{\pi E} \iint_{contact\ area} \frac{p(y',z')}{\sqrt{(y-y')^2+(z-z')^2}} dy'dz' \qquad (1)$$

where E and σ are Young's modulus and Poisson's ratio of the cell, respectively.

The configuration shown in Fig. 2(a), is considered for solving the contact problem between the cell and the arms, and finding consequent maximum arm displacement, when the cell touches the arms during transiting in the constriction channel.

The shape of the cell in the constriction channel is changed from a sphere to a cube-like shape. Without loss of generality of the design, dynamics of the cell movement and shape change is not considered in this work, and the cell shape is designed in a way that to be like cells in constriction channels in similar experiments [11]. The surface of the rectangle part of the arms in the constriction channel and the velocity of the cell should be large and low enough, respectively, to allow the cell completely interact with the arms and create maximum displacement of the arms for a specific cell. This maximum displacement is used to calculate electromagnetic response of the system.

Eq. (1) was used to find the force exerted on the contact area by the cell, for the first moment that the cell touches the arms and their displacement is approximately zero. This calculated force is used as an initial condition to simulate maximum displacement of the arms by using COMSOL software. It is assumed that the cell body and the arms, which are in contact, are isotropic and linearly elastic. Fig. 3 shows the arms displacement in X direction under the influence of the force exerted by a cell with Young's modulus of 0.73 kPa, Poisson's ratio of 0.49 and size of 11 µm, similar to MCF-10A [12]. It should be mentioned that the design of MAMS can be modified to be suitable for other types of cells with different characteristics.

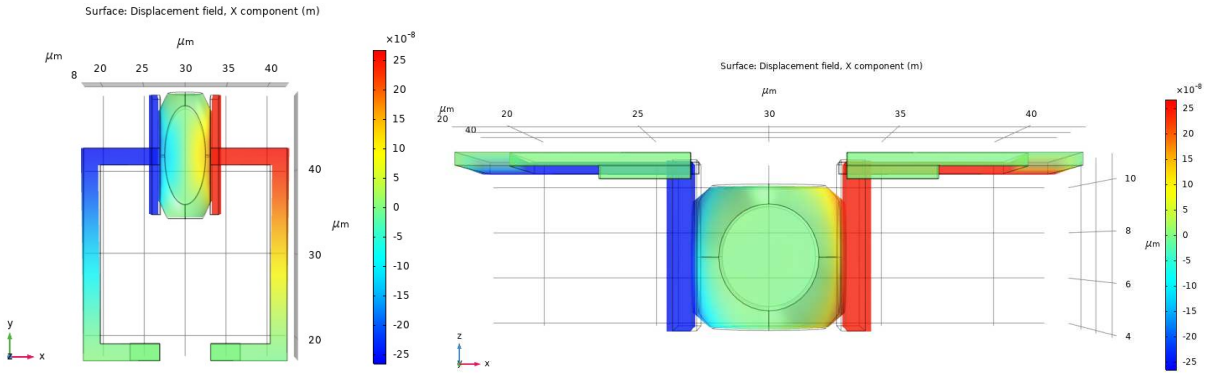

(a) (b)

Fig. 3. Arms displacement in X direction. (a) Top view (xy plane). (b) xz plane view.

When geometrical features of the two-gap SRR such as the size of the gaps are changed, electromagnetic response of MAMS is modified significantly, which demonstrates that high sensitivity detection is achievable using MAMS [13, 14]. In order to verify the expected functionality of MAMS and its performance, an electromagnetic simulation is performed using COMSOL software. Simulation results and analysis are presented in the next section.

III. Results & Discussion

To explore the THz characteristics of MAMS, a simulation based on finite difference time domain (FDTD) method by using COMSOL software is performed. Fig. 4 shows S_{21} parameter for zero arm displacement and different relative permittivities of the cell, 10, 20, 30, 40 and 50. It is assumed that the cell is not stiff and consequently would not displace the arms; this case provides a baseline for analysis and comparison of the results.

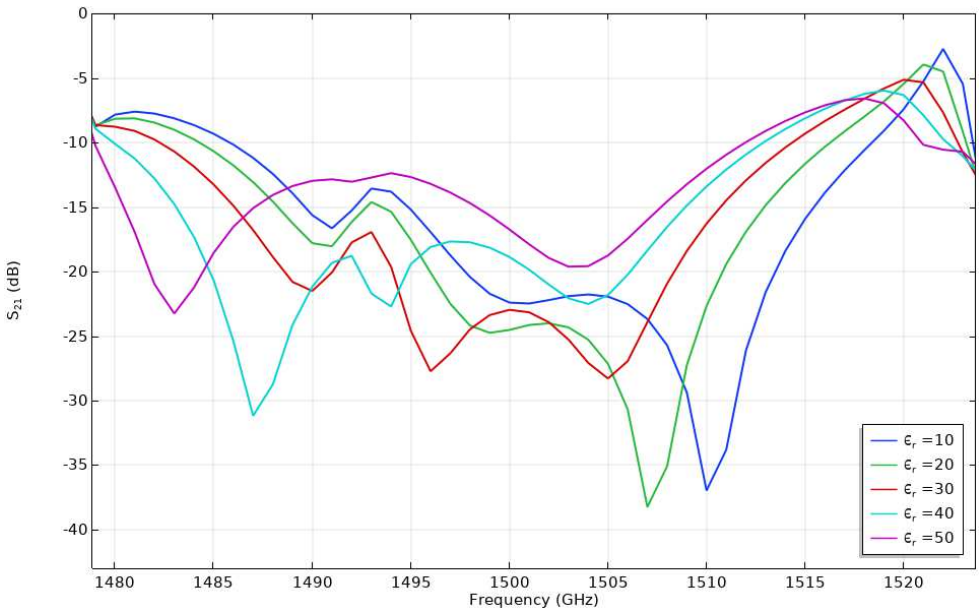

Fig. 4. S_{21} (dB) for zero arm displacement for different cell relative permittivities.

As can be seen in Fig. 4, by increasing ε_r, the resonance dips move toward lower frequencies, and resonance frequency shifts are remarkable. For example, by changing ε_r from 10 to 20, resonance frequency decreases from 1524 to 1507 GHz, or equivalently 17 GHz shift in resonance frequency. Presence of asymmetric geometrical features in MAMS such as the rectangle part of the arms and displaced arms allows MAMS to produce Fano resonances [15], which enhances the sensitivity of MAMS and Q value [16].

Fig. 5 shows the resonance frequency of MAMS as a function of arms displacement for different relative permittivities. With increasing ε_r, resonance frequency decreases, and as stated before, these changes in resonance frequency are significant, and the values of resonance frequency shift range from 4 GHz to about 40 GHz for specified values of arms displacement and cell relative permittivity, which shows excellent sensitivity of MAMS. The sensitivity of MAMS to arms displacement, which in fact is sensitivity to the cell stiffness, decreases for larger displacements.

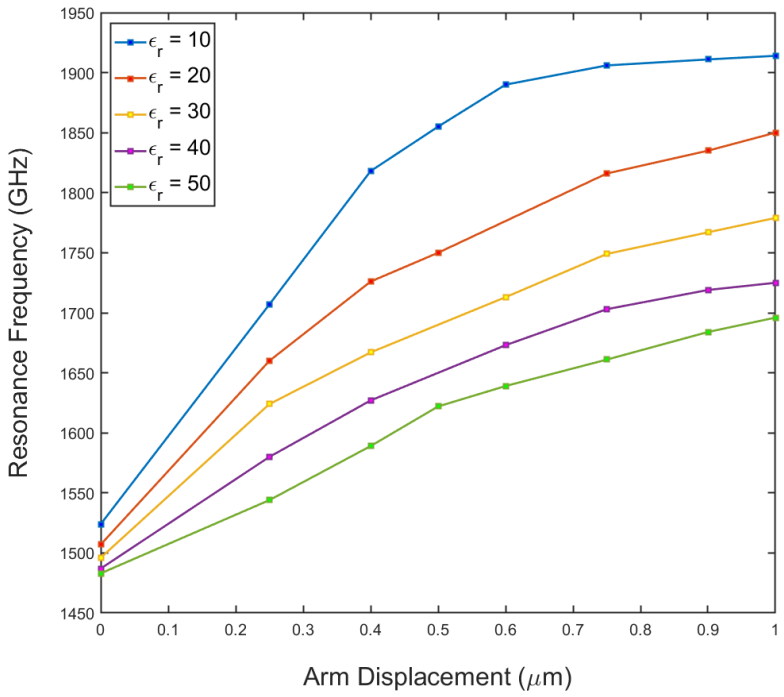

Fig. 5. Resonance frequency as a function of arm displacement for ε_r = 10, 20, 30, 40 and 50.

From a circuit theory perspective, a SRR can be considered as a resonator, which is coupled with illuminated electromagnetic wave. It can be modeled using an LC circuit and the resonance frequency of this LC circuit is as follows [17]:

$$f = \frac{1}{2\pi\sqrt{LC}} \tag{2}$$

where L and C are total inductance and capacitance at resonance frequency. The inductance L is formed by resonator loop, and varies with arms displacement. The capacitance C is formed by split gap in the SRR which contains the cell and carrier fluid. The effects of carrier fluid and fringing fields on capacitance is neglected. Therefore, the capacitance C can be considered as parallel plate capacitor and be written as: $C = \frac{\varepsilon_{cell} \times A}{split\ gap\ size + 2 \times arm\ displacement}$ where A is the area of the rectangle part of the arms in the constriction channel. Therefore, it would be an accurate

estimation that the cell dielectric properties affect electromagnetic response of MAMS, and especially resonance frequency shifts.

In this work, the relative permittivity sensitivity and displacement sensitivity, $\partial f(\varepsilon_{cell}, d)/\partial \varepsilon_{cell}$ and $\partial f(\varepsilon_{cell}, d)/\partial d$, are defined as dip frequency shift per relative permittivity unit (RPU) and displacement unit (μm), respectively. The displacement sensitivity is dependent on SRR design parameters, such as SRR geometrical features and properties of materials used in SRR. To analyze and improve sensitivity of MAMS, eq. (2) can be used. In this work, the displacement sensitivity reached 732 GHz/μm for $\varepsilon_r = 10$ and 265 GHz/μm for $\varepsilon_r = 50$; for larger displacements, these values decrease. For the cell relative permittivity, the sensitivity reached 113.6 GHz/RPU for 0.6 μm arm displacement. For larger and smaller displacements, the relative permittivity sensitivity decreases. For larger displacements, self-inductance of the SRR increases, which decreases frequency shift, and consequently decreases the relative permittivity sensitivity.

Excellent sensitivity of MAMS to both cell relative permittivity and stiffness, as distinct and independent biosignatures of a cell, enable us to characterize unknown cells during passing through MAMS with high sensitivity, and predict cell type and state accurately.

IV. Conclusion

A novel sensor for detecting and differentiating cells based on their stiffness and dielectric properties in a single assay presented. Both cell stiffness and relative permittivity, as two biosignatures of a cell, are reflected in the electromagnetic output characteristics of the device. In fact, the system is able to sense the effect of two independent cell properties in a single measurement. This device contains a

microfluidic constriction channel and a two-gap split ring resonator, which enables us to perform relevant assays with high sensitivity. The important advantage of this sensor is its high sensitivity; cells with close stiffness and relative permittivity values, which are their signatures, can be distinguished accurately. The current design can be easily modified to allow the sensor to be used for a variety of cancer cells as necessary. This label-free sensing method has the potential to be implemented in a lab-on-a-chip system for non-(electrical) contact cell detection and enumeration.

Conflicts of interest

There are no conflicts to declare.

References

[1] X. Ren, P. Ghassemi, J. Strobl and M. Agah, "Biophysical phenotyping of cells via impedance spectroscopy in parallel cyclic deformability channels",Biomicrofluidics, vol. 13, no. 4, p. 044103, 2019.

[2] Masaeli, M., Gupta, D., O'Byrne, S. et al. Multiparameter mechanical and morphometric screening of cells. Sci Rep 6, 37863 (2016). https://doi.org/10.1038/srep37863.

[3] J. Hwang et al., "Cell Deformation by Single-beam Acoustic Trapping: A Promising Tool for Measurements of Cell Mechanics", Scientific Reports, vol. 6, no. 1, 2016. Available: 10.1038/srep27238.

[4] Choi, G., Nouri, R., Zarzar, L. et al. Microfluidic deformability-activated sorting of single particles. Microsyst Nanoeng 6, 11 (2020). https://doi.org/10.1038/s41378-019-0107-9.

[5] Xue, C.; Wang, J.; Zhao, Y.; Chen, D.; Yue, W.; Chen, J. Constriction Channel Based Single-Cell Mechanical Property Characterization. Micromachines 2015, *6*, 1794-1804. https://doi.org/10.3390/mi6111457.

[6] Ghassemi, P., Ren, X., Foster, B.M., Kerr, B.A., Agah, M., Post-enrichment circulating tumor cell detection and enumeration via deformability impedance cytometry, Biosensors and Bioelectronics (2019), doi: https://doi.org/10.1016/j.bios.2019.111868.

[7] A. K. Horestani, C. Fumeaux, S. F. Al-Sarawi and D. Abbott, "Displacement Sensor Based on Diamond-Shaped Tapered Split Ring Resonator," in IEEE Sensors Journal, vol. 13, no. 4, pp. 1153-1160, April 2013, doi: 10.1109/JSEN.2012.2231065.

[8] Awang, R. A., Tovar-Lopez, F. J., Baum, T., Sriram, S., & Rowe, W. S. T. (2017). Meta-atom microfluidic sensor for measurement of dielectric properties of liquids. Journal of Applied Physics, 121(9), 094506. https://doi.org/10.1063/1.4978012.

[9] M. J. Puttock and E. G. Thwaite, Elastic Compression of Spheres and Cylinders at Point and Line Contact, National Standards Laboratory Technical Paper No.25, Melbourne, Australia; 1969.

[10] J. Prescott, Applied Elasticity, London: Longmans Green & Co., 1924.

[11] X. Ren, P. Ghassemi, H. Babahosseini, J. Strobl and M. Agah, "Single-Cell Mechanical Characteristics Analyzed by Multiconstriction Microfluidic Channels", ACS Sensors, vol. 2, no. 2, pp. 290-299, 2017.

[12] C. C V, A. Ahmed Mubeen, S. Chaudhary and A. Barathwaj R, "Dynamic analysis of MCF-10A and MCF-7: A simulation approach", Vibroengineering PROCEDIA, vol. 30, pp. 126-132, 2020.

[13] Zhao, X., Duan, G., Li, A. et al. Integrating microsystems with metamaterials towards metadevices. Microsyst Nanoeng 5, 5 (2019). https://doi.org/10.1038/s41378-018-0042-1.

[14] W. Zhang et al., "Metafluidic metamaterial: a review", Advances in Physics: X, vol. 3, no. 1, p. 1417055, 2018.

[15] W. Su, Y. Liu and B. Chen, "Multiple Fano resonances in asymmetric rectangular ring resonator based on graphene nanoribbon", Results in Physics, vol. 17, p. 103121, 2020.

[16] Z. Geng, X. Zhang, Z. Fan, X. Lv and H. Chen, "A Route to Terahertz Metamaterial Biosensor Integrated with Microfluidics for Liver Cancer Biomarker Testing in Early Stage", Scientific Reports, vol. 7, no. 1, 2017.

[17] M. Moniruzzaman, M. Islam, N. Misran, M. Samsuzzaman, T. Alam and M. Chowdhury, "Inductively tuned modified split ring resonator based quad band epsilon negative (ENG) with near zero index (NZI) metamaterial for multiband antenna performance enhancement", Scientific Reports, vol. 11, no. 1, 2021.